Analysis of Roller Compaction Pressure Distribution in Automated Dry Fibre Placement

Shimin Lu*, Anthony Evans, Thomas Turner

Composites Research Group, Faculty of Engineering, University of Nottingham, NG7 2RD, United Kingdom

Abstract

Automated Dry Fibre Placement (ADFP) is a version of Automated Fibre Placement (AFP) where prepreg tapes are substituted with dry fibre tapes. In this process, a uniform compaction pressure applied by a compaction roller is required to manufacture preforms with consistent quality. In this paper, a finite element model is developed to analyse the roller-applied pressure on the fibrous reinforcement bed. The model has been validated by using a pressure sensitive film. The influence of roller material, tool curvature and substrate thickness on the pressure distribution are investigated. Increasing tool curvature leads to a decrease in compaction pressure uniformity using the same compaction force. Force input target bounds for different rollers on tools with different curvatures are determined using the model. It is found that softer rollers show large force control window and suitability for tools with higher curvature. Thick substrates exhibit large deformation which could increase complexity for force control strategies.

Key words: automated dry fibre placement (ADFP), compaction roller, pressure distribution, force control

1. Introduction

Composite materials are widely used in the aerospace industry due to their high specific stiffness and strength. Automated fibre placement (AFP) is an efficient technique to manufacture large aerospace composite components because the labour cost and material waste is reduced while the layup speed, accuracy and reproducibility are increased when compared with the hand layup technique [1]. In the AFP process, prepreg materials are compressed on the tool or the substrate layers by a compaction roller mounted on a robotic arm or gantry system. The compaction force applied to the roller influences the quality of the parts and needs to be precisely controlled. The tack between prepreg materials and the tool partially determines the quality of the parts and is strongly influenced by the compaction force [2-5]. The intimate contact and bonding between adjacent layers are influenced by the compaction force [6-8]. Mechanical properties, such as the interlaminar shear strength, facture toughness and bending modulus, of AFP-manufactured laminates are influenced by the compaction force [9-13]. Physical characteristics such as cured ply thickness and the formation of defects, such as wrinkles and voids [14-16] are also influenced.

The roller transfers the compaction force applied by the machine to the compaction pressure on the plies. A high level of uniformity of compaction pressure is required in the AFP process to achieve optimal quality. Several researchers have analysed rollers and sought to optimise the roller geometry to achieve a uniform compaction pressure. For compaction on flat tools, the uniformity of pressure generated by solid rollers with wide range of modulus, diameters and lengths is higher than 80% [17] but perforated rollers have been shown to reduce the uniformity of the pressure distribution compared with solid rollers and this reduction could lead to defect generation [15, 18]. For compaction on non-flat tools, the pressure uniformity of rollers could be reduced from 89% to 16% [17]. This non-uniform pressure distribution restricts the application of AFP on parts with high curvature. The roller geometry therefore needs to be optimised to tackle this issue. For simple non-flat tools such as tools with single curvature or ramps, FE models have been built to investigate the influence of roller material and geometry on the pressure uniformity [17, 19, 20]. It is concluded that soft, compliant rollers generate a larger contact area and a more uniform pressure distribution than stiff rollers. In addition, rollers with larger diameter and shorter length can generate more uniform pressure distribution. Roller geometry selection criteria have been established based on the deformability of rollers on surfaces with single curvature [21]. For complex irregular tools, a theoretical model has been built to investigate the pressure distribution applied by the compaction roller [22]. This model has been used to analyse a segmented roller and it is found that for irregular tools, a segmented roller could generate a more uniform pressure than a solid roller [23]. Besides optimising the geometry or material of rollers, the pressure uniformity can also be improved by dynamically controlling the yaw and roll angle of the head based on the tool geometry [16]. These works focus on situations where the roller is compacted on either the tool surface or with one layer of prepreg between them. No research has been found investigating the roller pressure distribution on other common situations in the AFP process, such as thick prepreg substrates and substrates with gaps and overlaps.

*Corresponding author. Email address: shimin.lu@nottingham.ac.uk

Automated dry fibre placement (ADFP) is a relatively new technique to manufacture large aerospace components [24]. The ADFP process uses similar deposition hardware as AFP but substitutes a bindered dry fibre reinforcement for the prepreg materials. ADFP-manufactured preforms are then transferred to an impregnation process such as resin infusion and resin transfer moulding (RTM). Compared with the hand layup technique, ADFP shares many of the advantages of AFP and laminates manufactured by ADFP with vacuum resin infusion process show a 9% increase of fibre volume fraction and decreases of porosity and thickness variation than laminates manufactured by manual layup with vacuum resin infusion [25, 26]. Compared with AFP, the manufacturing costs of ADFP are theoretically reduced because of the use of low-cost raw materials and out-of-autoclave process. Bindered dry fibre reinforcement used in ADFP has no matrix resin, which could result in a decrease in downtime events and repair times for the deposition machine and an increase of laydown rates comparing with AFP [27].

Like AFP, in ADFP the compaction force could also influence the bonding of dry fibre tape to the tool and adjacent dry fibre layers. Compaction pressure is even more important in ADFP than AFP because the compaction pressure directly influences the fibre volume fraction of the preforms which determines the mechanical properties of the final laminates. Uniformity of compaction pressure is required in the ADFP to manufacture preforms with consistent fibre volume fraction. In dry fibre tow or fabric compaction testing, the compaction pressure and the fibre volume fraction shows a power-law relationship [28]. However in ADFP, it has been shown that high compaction pressure can lead to lower fibre volume fraction of the preforms [29, 30]. It is surmised that this reduction is caused by the high compaction-induced through-thickness shear stress which leads to the breakdown of the binder bond and the subsequent deconsolidation of the preforms. However, this assumption needs further research on the stress field of the dry fibre-roller interaction.

Using dry fibre reinforcement in automated placement process also brings issues. Dry fibre reinforcement exhibits a large geometry change under process conditions. Thickness reduction of dry carbon fibre tows has been found to be higher than 20% under sufficient compaction [28, 29] while that of thermoset prepregs under AFP process conditions has been found to be less than 10% [31]. In practice, however, commercial materials for ADFP are highly engineered to give consistent in-process performance in the through-thickness direction. But the large thickness change still exists and it can bring difficulties for ADFP force control. Commercial deposition hardware tends to include some built-in compliance in the form of a pneumatic cylinder in order to maintain a roughly constant compaction force. This compliance introduces uncertainty in that the height of the deposition head is not known, there may also be issues in responding to rapid changes in thickness or tool geometry.

In this paper, a finite element (FE) model with a non-linear elastic compaction material model is developed to investigate the pressure distribution applied by compaction roller on dry carbon fibre substrates. The properties of carbon fibre tapes and the roller materials are characterised experimentally. The FE model is validated by experiments using pressure sensitive film and is then used to investigate the influence of the roller material and tool curvature on the uniformity of the compaction pressure. A target pressure requirement is chosen and force input bounds for tools with different curvature are determined. The influence of substrate thickness on compaction pressure distribution and compaction force control method is also investigated.

2.Experimental work

Materials:

24K TX1100 (Solvay) bindered carbon fibre tapes with a width of 6.35 mm, a nominal thickness of 0.275 mm and an areal weight of 212 g/m^2 shown in Figure 1 were used in this research. The tapes have binder particles in one surface and a carbon veil on the other surface [26, 32]. The roller is made from four parts: a rubber cover, a sleeve, a shaft and two bearings as shown in Figure 2. Three materials: silicone rubber (Polycraft FS30) with the shore A hardness of 28, silicone rubber (Easycomposites AS40) with the shore A hardness of 40, and polyurethane rubber (DuroFlex 95) with the shore A hardness of 95 were used to manufacture the roller cover. The hardness level is comparable with the hardness level of rollers used in commercial AFP machines [30, 33]. The sleeve and shaft were manufactured from steel.
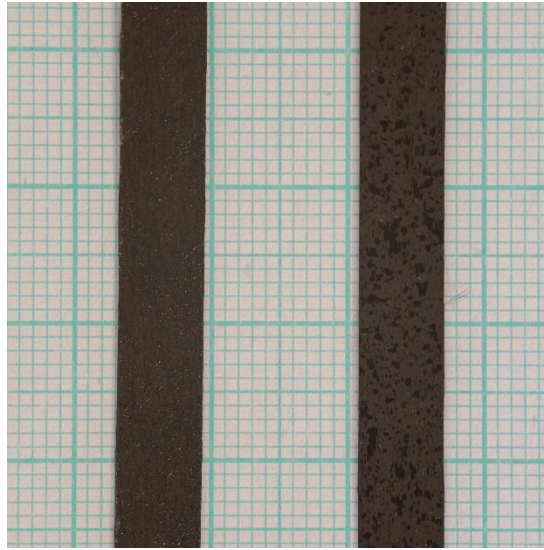
Figure 1 Carbon fibre tapes used in this paper showing upper and lower surfaces (1 mm minor grid spacing)
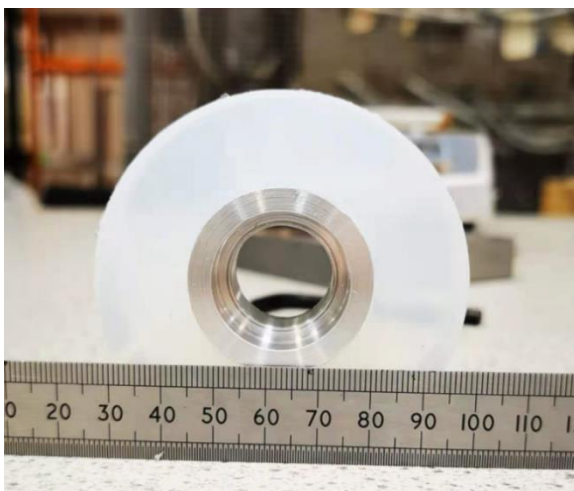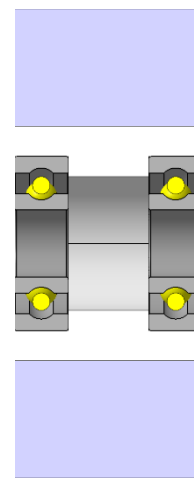
(a)   (b)

Figure 2 Compaction roller (a) Manufactured roller (b) Cross-section view of roller in CAD

Compaction test for dry carbon fibre tapes

The through-thickness properties of dry carbon fibre tapes were characterised by compaction testing. Each test comprises a single piece of tape with a length of 60 mm and a width of 6.35 mm. The test was conducted on an Instron 5969 universal testing machine with two parallel circular platens as shown in Figure 3. The compaction force was 500 N and the loading rate was 0.3 mm/min. Two LVDT's (MICRO-EPSILON D6/02500ARA-L10) were used to measure the thickness of the tape and the average value of the two sensors was used to calculate the fibre volume fraction of the tape using equation (1). The initial fibre volume fraction of the tape was calculated when the load was 5 N.
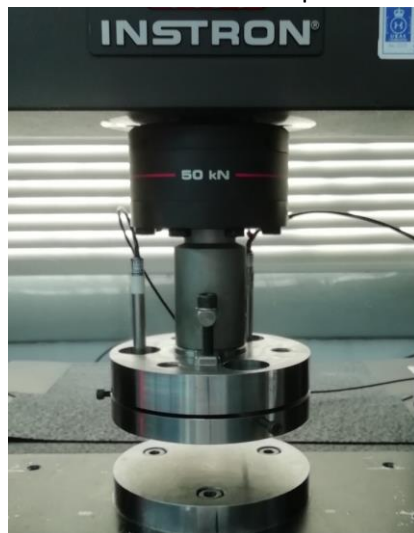
Figure 3 Dry fibre tapes compaction testing experimental apparatus

$$V_f = \frac{A_F}{\rho_f t} \qquad (1)$$

Where A_F is the areal weight of the carbon fibre tapes. ρ_f is the fibre density. t is the thickness of the tape.

The compaction curve of the tapes was then obtained as shown in Figure 4. A power law formula was used to fit the compaction curve and the power law parameters were used in the finite element model as explained in section 3.
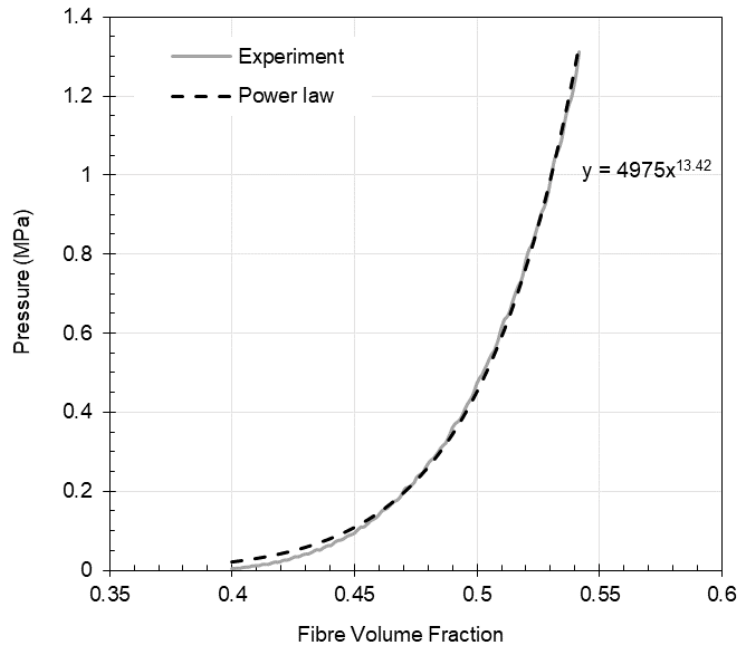
Figure 4 Compaction curve of carbon fibre tapes from experimental results with power law fitted curve

Roller manufacturing and characterisation testing

For the two silicone rubber covers, the silicone rubber and the cure catalyst were mixed thoroughly with the weight ratio of 10:1 and the mixture was then degassed in a vacuum chamber. The degassed mixture was filled into the roller mould containing the steel sleeve. They were transferred to an oven with a temperature of 50 °C. The silicone rubber was then cured in the oven for an hour. The rubber cover with the co-moulded sleeve was then demoulded. For the polyurethane rubber cover, the polyurethane part A and part B were mixed thoroughly with the weight ratio of 1:1 and the manufacture proceeded as above. The diameter of the rollers is 70 mm and their width is 28 mm. The diameter of the sleeve is 35 mm. The dimension of three rollers is same as the dimension of the roller used in a lab-scale ADFP rig to lay down four tows each course [34]. The diameter of the rollers is same with the diameter of rollers in commercial AFP machines [30, 33]. The rollers were installed on an Instron 5966 universal machine with a fixture as shown in Figure 5. The rollers were compacted on a flat rigid surface with a compaction force of 700 N and a load rate of 2 mm/min. The roller was rotated 90° after one test and four repeats were conducted in total to check the influence of the material uniformity of the roller. The load-displacement curves of the rollers were thus obtained.
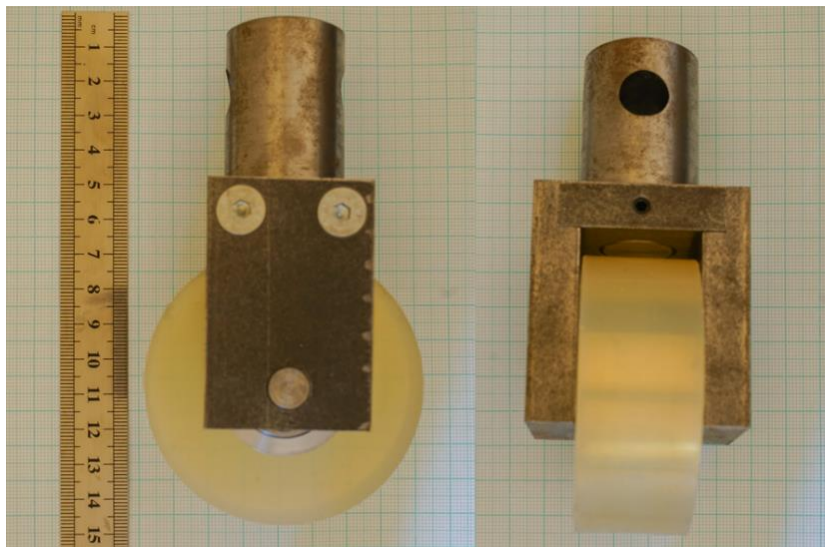
Figure 5 Compaction roller with fixture

Roller compaction on fibres testing

Static roller compaction testing on a fibre bed was conducted in this research. In the real ADFP process, the roller is rotating dynamically but at the velocities of interest the roller rotation has a negligible influence on the value of compaction pressure [17]. For analysis of compaction pressure, static testing can therefore generate valuable results. Five TX1100 tows with a length of 100 mm were placed on a steel flat tool with no visible gaps between them. The surfaces with the binder particles were adjacent to the tool surface. The width of the roller is slightly larger than the width of one course which contains four tows. When depositing the current course, the extra width of the roller compacts the previous course. Thus, five tows in total are compacted during the deposition. Pressure sensitive films were placed on top of the five tows. The roller was compacted on the centre of the tapes covered with the pressure sensitive films by an Instron 5966 universal machine. The experimental setup is shown in Figure 6. Three load levels were tested on the three rollers as shown in Table 1. The load rate was set to achieve the load level in around 5 s and the load was then held in 2 minutes according to the pressure sensitive film manual. The pressure distribution was then measured by the pressure sensitive films.
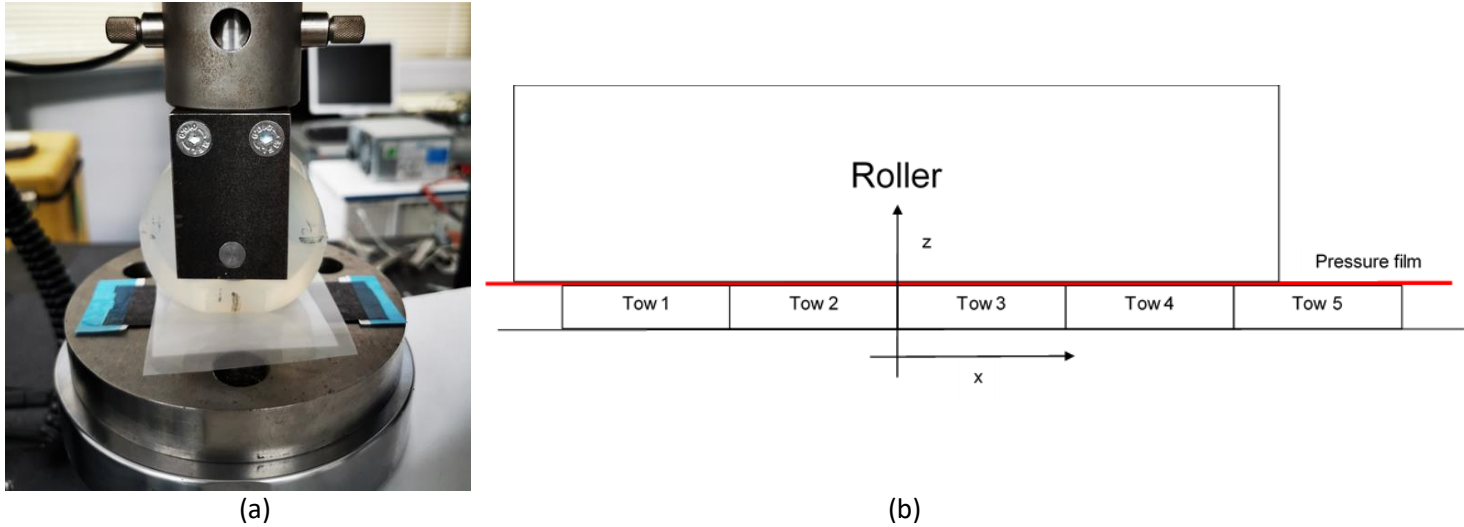
(a)   (b)

Figure 6 Experimental setup for compaction on fibres test (a) machine setup (b) illustration of the relative location of the roller and fibre tows

Table 1 Forces used to determine compaction behaviour

Roller Hardness (HA)	Load level 1 (N)	Load level 2 (N)	Load level 3 (N)
28	100	250	400
40	70	200	380
95	20	30	50

Compaction pressure measurement method

Fujifilm LLLW pressure sensitive films with a measurement range from 0.2 MPa to 0.6 MPa were used. The films display a different density of red colour after being compressed. The procedure developed by He *et al*. and Jiang *et al*. [22, 23] was used to obtain the pressure values from the pressure film. The manufacturer manual which has all sample red colour rectangular patterns and their colour density ρ was scanned by a flatbed scanner. The average grayscale a of each sample colour rectangular pattern is calculated by Matlab. The relationship between the sample colour density ρ and their average grayscale a is then fitted as $\rho = f(a)$. The relationship between the sample colour density ρ and the pressure value P is provided as a curve by the manufacturer and can be fitted as $P = g(\rho)$. The relationship between the average grayscale a and the pressure value is then obtained as $P = g(f(a)) = F(a)$. The pressure sensitive films were scanned alongside a paper scale in a flatbed scanner. The grayscale of each pixel in the scanned picture is calculated by Matlab and then the pressure distribution is calculated by using the relationship $P = F(a)$. Figure 7 shows the compacted pressure sensitive films and the pressure results. It is shown that the pressure values are scattered instead of continuous due to the inhomogeneous red dots in the pressure sensitive films. To reduce this inhomogeneity, the average greyscale value of all pixels in an area of 0.5 mm by 0.5 mm instead of the greyscale of each pixel is used to calculate the pressure value for the whole area, since the relationship $P = F(a)$ is obtained using average grayscale values of sample colours. Values below 0.2 MPa are deleted and the values above 0.6 MPa are set to 0.6 MPa due to the measurement range of the film. Figure 8 shows the comparison of pressure values along the

centreline of the tow in y direction (the dash line in Figure 7) obtained by raw data and averaged data. The experimental pressure values in following sections are obtained using the averaging method described above.
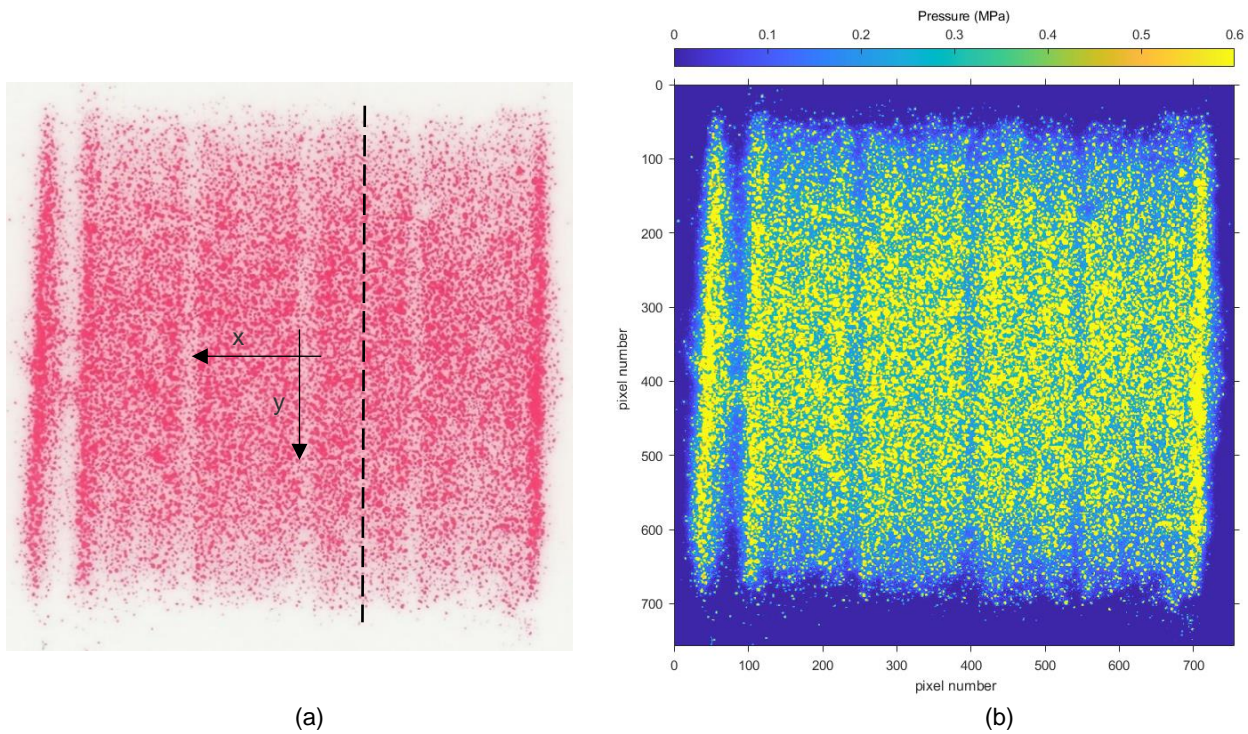
(a)   (b)

Figure 7 Pressure film and pressure results (a) scanning picture of pressure sensitive film (b) calculated pressure values from Matlab
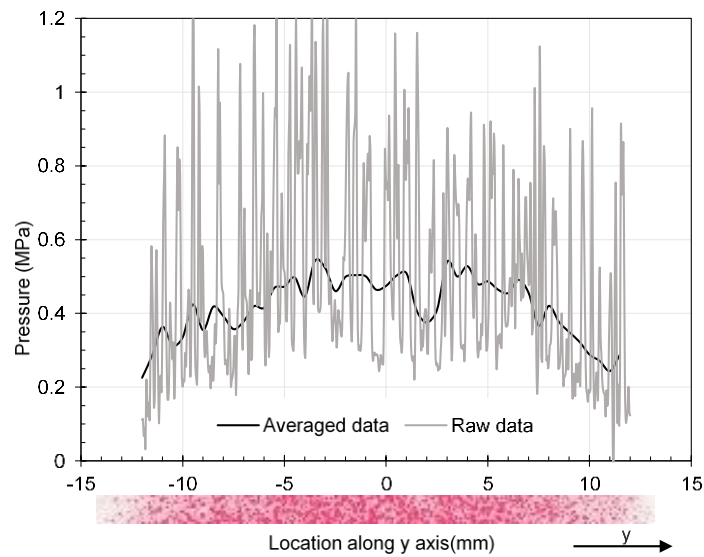
Figure 8 Averaged pressure results along tow centreline in y direction (the dash line in Figure 7) from pressure sensitive film

3.FE model development

FE model setup

A finite element model of roller compaction on dry carbon fibres was developed using Abaqus/CAE. The model consists of four parts: a sleeve, a tool, a rubber cover and dry carbon fibre tapes. Because of the symmetry of the structure and the load, half of the structure and the load are used during the FE analysis with a symmetric boundary condition as shown in Figure 9. The sleeve with a diameter of 35 mm is modelled as a rigid body and the compaction force is applied to its reference point. The tool is constrained as a fixed rigid body. The dimension of the half tool is 45 mm × 40 mm. The interactions between the rubber cover and the sleeve, between the dry fibre tapes and the tool are modelled as tie constraints. The contact between the rubber cover and the dry fibre tapes and the contact between the rubber cover and the tool are modelled as hard contact conditions. The degrees of freedom of displacement of the rubber cover except in the through-thickness direction are constrained to zero and the 8-node linear brick C3D8 element is chosen for the rubber cover. For the dry fibre tapes, five tows are modelled as one part with the dimensions 40 mm × 31.75 mm × 0.275 mm and again the C3D8 element is chosen. The relative location of the roller and fibre tows is the same as the experimental setup shown in Figure 6 (b). After a mesh size dependency analysis, the mesh size for the

top and bottom half rubber cover is chosen to be 2 mm and 0.75 mm respectively. The mesh size for the dry fibre tapes is chosen to be 0.18 mm. A modified transversely isotropic elastic material model with a nonlinear response in the through-thickness direction based upon the method developed by Lin and Sherburn [35, 36] is used for the dry
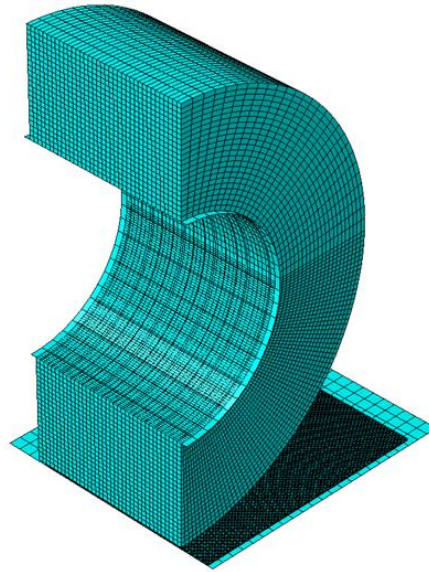
fibre tapes, the details are given in the material models section.

Figure 9 FE model setup for roller compaction on a layer of dry carbon fibre

Material models

For the silicone rubber, a linear isotropic elastic material model is chosen. The material property parameters are obtained by fitting the load-displacement curve from the roller characterisation testing as shown in Figure 11.

The compaction mechanism of the dry fibres is complicated and includes elasticity, plasticity, relaxation, viscoelasticity and cyclic effects [28]. This model focuses on the quasi-static compaction pressure distribution when the dry fibre tapes are compacted by the roller and only the elasticity is currently considered in this model. In the longitudinal fibre direction, the modulus is modelled as a linear function of the fibre volume fraction V_f of the dry fibre tapes [35]. In the compaction testing conducted by the authors and in literature [37], the length of the dry fibre tow shows no change after the compaction. Thus, the values of the Poisson's ratio v_{12}, v_{13}, v_{31} and v_{21} are assumed to be zero. The stress in the longitudinal direction is then described by the following equation:

$$\sigma_1 = E_0 V_f \varepsilon_1 \quad (2)$$

Where E_0 is the modulus of the carbon fibre. V_f is the fibre volume fraction of the dry fibre tapes.

In the through-thickness direction, the response is nonlinear. When analysing the compaction experimental results, the relationship between the compaction pressure P and the fibre volume fraction V_f is fitted using a power law with two parameters a and b according to the following equation:

$$P = a V_f{}^b \quad (3)$$

The through-thickness stress σ_3 has the same value as the compaction pressure P but with a minus sign:

$$\sigma_3 = -P \quad (4)$$

The fibre volume fraction V_f is represented as a function of through-thickness strain ε_3 [36]:

$$V_f = \frac{V_{f0}}{exp\,(\varepsilon_3)} \quad (5)$$

Where V_{f_0} is the initial fibre volume fraction of the dry fibre tapes before compaction. Substituting equation (4) and (5) to (3), the following equation is obtained:

$$\sigma_3 = -a \left(\frac{V_{f0}}{\exp(\varepsilon_3)}\right)^b \quad (6)$$

In compaction testing, the Poisson's ratio v_{23} shows a nonlinear relationship with the through-thickness strain ε_3 and its value is typically lower than 0.1 [37, 38]. For simplicity, its value is assumed to be zero in this model. The through-thickness stress σ_3 is then the function of only ε_3 as shown in equation (6). The transverse isotropic model is used, and the in-plane transverse direction shows the same response as the through-thickness direction. The stress σ_2 is defined according to the following equation:

$$\sigma_2 = -a \left(\frac{V_{f0}}{\exp(\varepsilon_2)}\right)^b \quad (7)$$

For the shear stresses, the shear moduli G_{12}, G_{13}, G_{23} are described by linear elastic material models. The material property inputs are shown in the Table 2. E_0 is obtained from the fibre manufacturer datasheet. G_{12} and G_{13} are obtained from literature [35]. Data for G_{23} is limited but it has minimal influence on the compaction response. Thus G_{23} assumed to be a small value of 2 MPa. V_{f_0}, a, b are generated from the experiments described in section 2. This dry fibre material model is implemented using the subroutine UMAT in Abaqus.

Table 2 Input values for the material model of the dry fibre tapes

Input	Symbol	Value
Power law parameter	a	4975
Power law parameter	b	13.42
Initial Fibre volume fraction	V_{f0}	0.3997
Modulus of fibre	E_0	290 GPa
Poisson's Ratio	v_{12}, v_{13}, v_{23}	0
In-plane shear modulus	G_{12}, G_{13}	5 MPa
Transverse shear Modulus	G_{23}	2 MPa

Compaction pressure uniformity calculation

Nodal contact pressure values are used to calculate compaction pressure uniformity. Pressure uniformity u is calculated using the following equation.

$$u = 1 - \sqrt{\frac{1}{n}\sum_{i=1}^{n}\left(\frac{p_i - \bar{p}}{\bar{p}}\right)^2} \quad (8)$$

Where n is the number of nodes. p_i is the contact pressure value at the node i . $\bar{p}$ is the average contact pressure value of all nodes.

FE model testing:

A flat tool and tools with radius of curvature of 20 mm, 30 mm, 50 mm, 100 mm, 200 mm and 500 mm are chosen to investigate the influence of tool geometry on the pressure distribution uniformity. The tool and dry fibres have a single curvature and the direction of the curvature is as shown in Figure 10. The relative location of roller and dry fibre tows is shown in Figure 6 (b). The boundary between tow 2 and tow 3 is positioned at the highest point of the tool. Three sets of material properties for the rubber cover materials are used to investigate the influence of the roller material. These are chosen to fit the load-displacement curves obtained from the experiments described above. Investigation of thick dry fibre substrates is also conducted. The thickness of the dry fibre substrates was chosen as 0.275 mm (1 layer), 2 mm, 5 mm and 10 mm. The model is slightly simplified for the thick dry fibre substrate cases to speed up the simulation. The width of the dry fibre substrate in the x direction is set as the same width as the width of the roller. Coarser mesh sizes are chosen for thick substrates. Mesh sizes of 0.4 mm, 0.5 mm and 0.7 mm are used for dry fibre substrates with the thickness of 2 mm, 5 mm and 10 mm respectively.
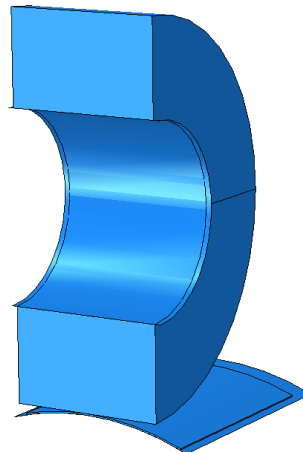
Figure 10 FE Model setup of roller compaction on dry carbon fibre with single curvature tools

4.Results and Discussion

Fibre and rubber material properties characterisation

Figure 4 shows the experimental compaction curve of the TX1100 carbon fibre tows and the power-law fitted curve. A power-law equation $P = 4975\, V_f^{13.42}$ is the best fit for the experimental curve, this was obtained by using a nonlinear least squares method provided by the Matlab curve fitting toolbox. This results in an R squared value of 0.998.
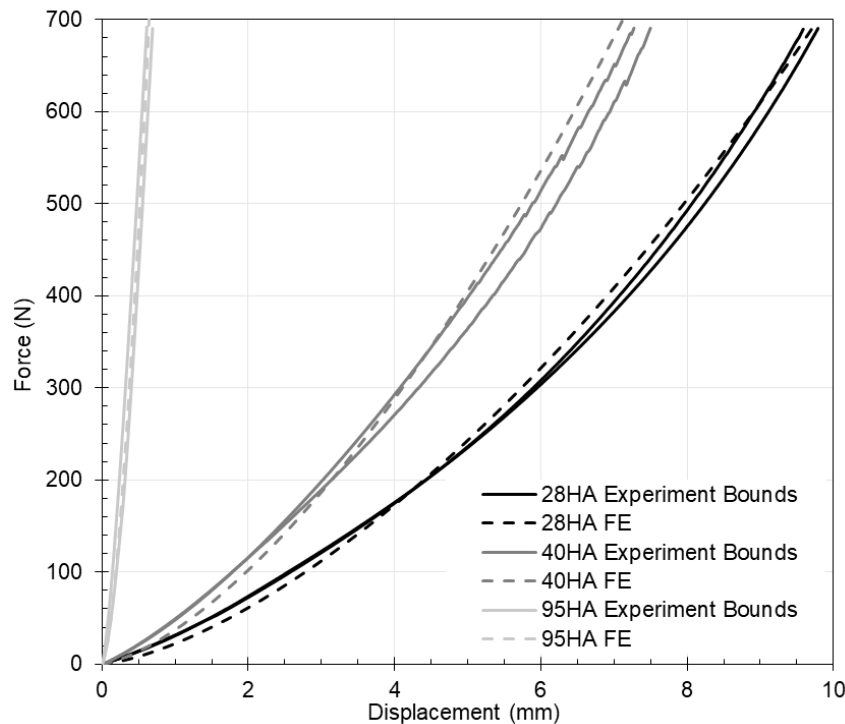
Figure 11 Load displacement curves of three rollers from experimental and FE results (experimental curves show upper and lower bounds based on four repeats)

Figure 11 shows the load-displacement curves of the rollers from the experiments and the FE model with fitted linear elastic material properties. It is shown that the linear elastic model used for the rubber cover can provide good agreement with the experimental data. The material properties used for the three rollers are shown in Table 3. It is found that the hardest 95 HA roller had a very low displacement compared to the softer rollers under the same compaction force. This low displacement makes precise force control difficult, particularly when the positional accuracy of deposition head is limited.

Table 3 Material properties for the rollers

Roller Hardness (HA)	Modulus (MPa)	Poisson's Ratio
28	0.165	0.475
40	0.275	0.475
95	12.5	0.475

Roller compaction on fibre testing results and FE model validation

Table 4 shows the compaction pressure distribution of the three rollers with the three load levels from Table 1. Peak pressure (a pressure spike) is observed at the area around the roller edges. Pressure drops are found between adjacent tows although the tows were butted together without visible gaps. It is found that for the same load level, the hardest 95 HA roller generates the smallest contact area with a highly non-uniform pressure, which is not desirable for the requirements of the manufacturing process. Thus, 95 HA roller is not analysed in later sections.

Table 4 Compaction pressure distribution results under three different load level for three rollers

Roller Hardness (HA)	Load Level 1	Load Level 2	Load Level 3
28			
40			
95			

(a)

(b)
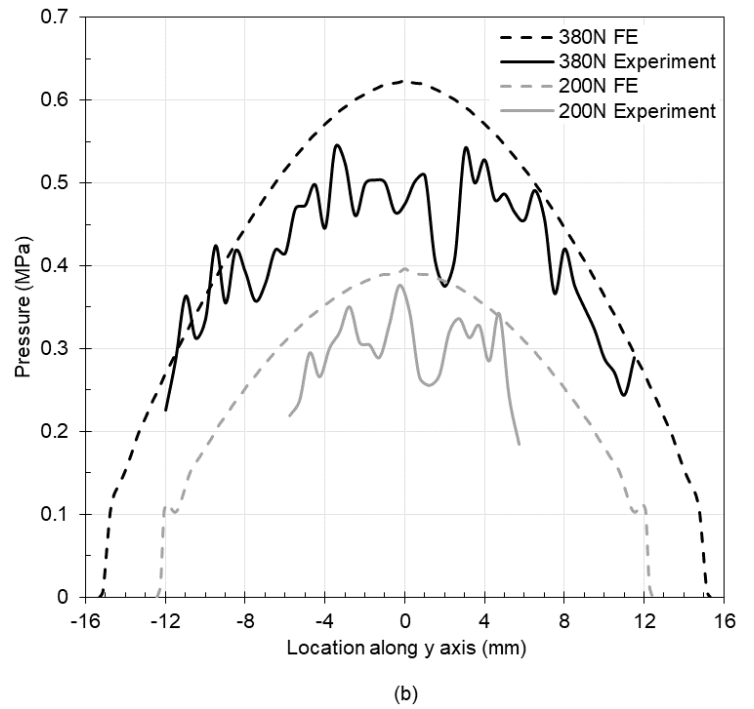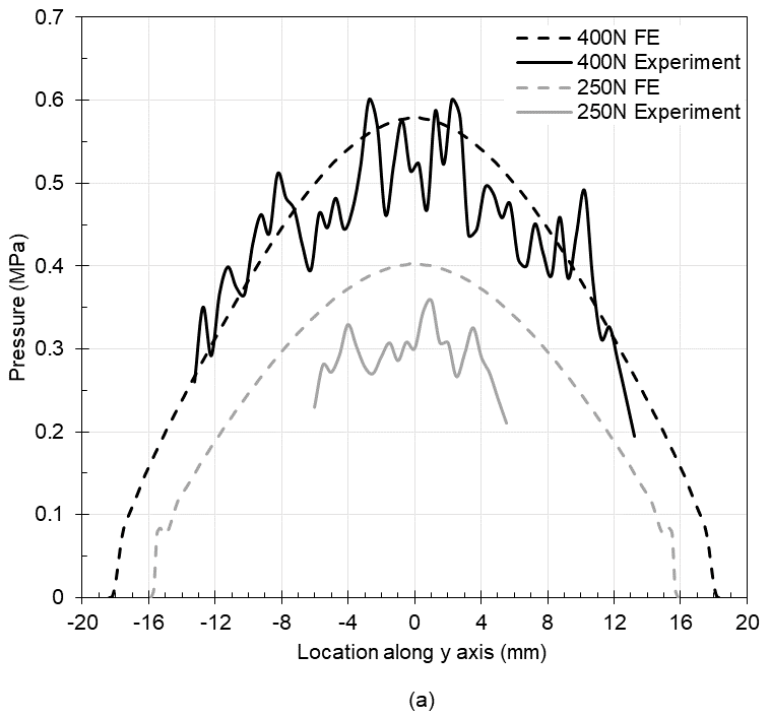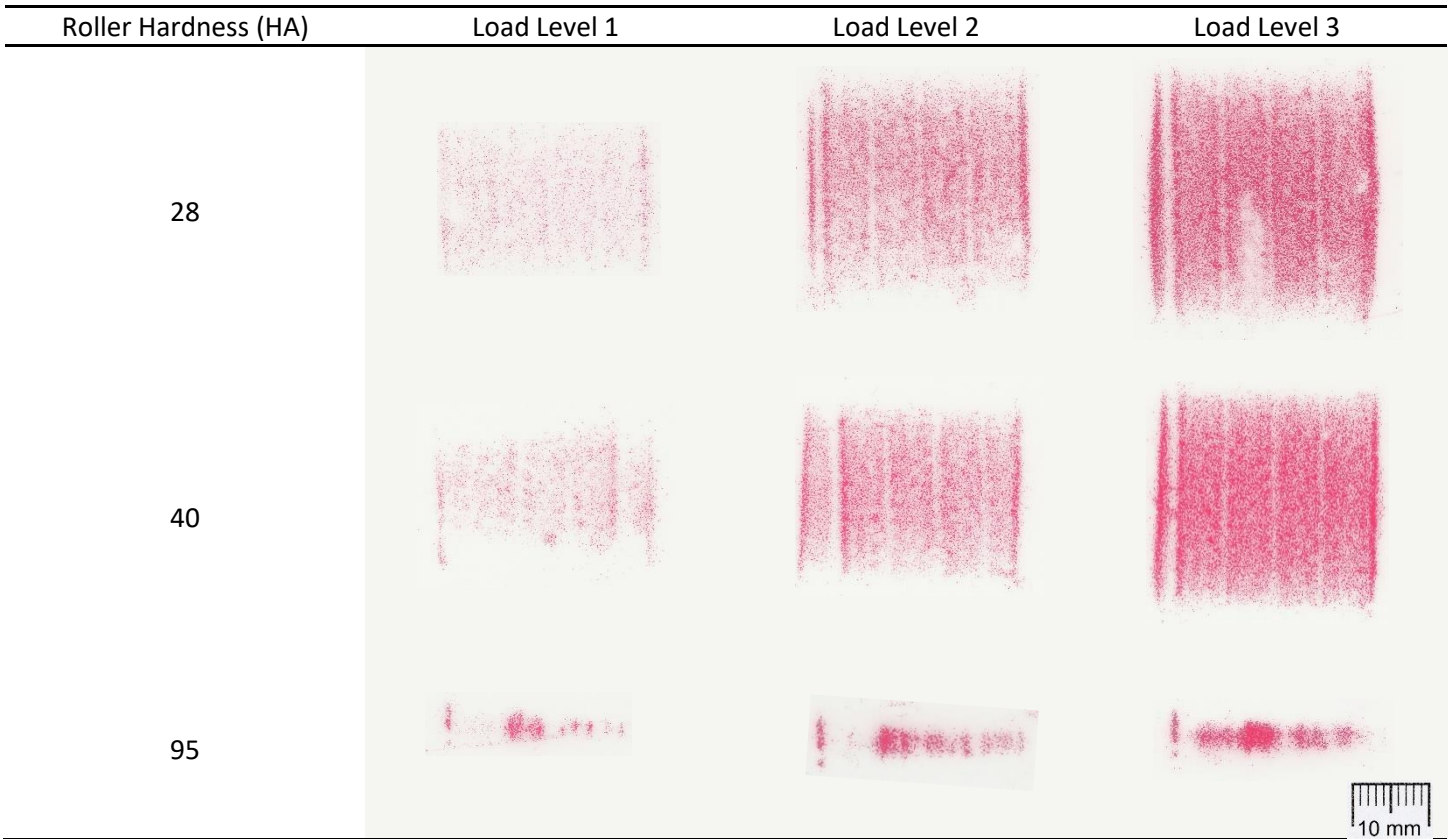
Figure 12 Compaction pressured distribution along tow centreline in y axis from experimental and FE results (a) 28 HA roller (b) 40 HA roller

Figure 12 shows the compaction pressure distribution along the tow centre line in y direction from the pressure sensitive film measurement compared to the FE model results. The pressure from load level 1 is smaller than the measurement range of the pressure film so the pressure distribution from load level 2 and load 3 only are compared with the FE results. It is shown that the experimental curves have significant fluctuations due to the inherent variability of the pressure sensitive film, and the FE result curves have good agreement with experimental curves although the pressure values show low level differences. The ±10% measurement error of the pressure sensitive film, the pressure calibration method and the averaging method all contribute to the pressure fluctuations and differences observed.

Influence of roller material on roller deformation and contact area

Table 5 shows the roller deformation and the contact area of 28 HA and 40 HA rollers under a compaction force of 400 N. It is found that under same compaction force, the 40 HA roller exhibits lower deformation and smaller contact area compared with the 28 HA roller hence the compaction pressure from 40 HA roller is higher than that from 28 HA roller.

Table 5 Simulation results of the roller deformation and the contact area of 28 HA, 40 HA roller under a compaction force of 400 N

Roller	Roller Deformation	Contact Area
28 HA		 26.7 mm × 18.2 mm
40 HA		 26.7 mm × 16.0 mm
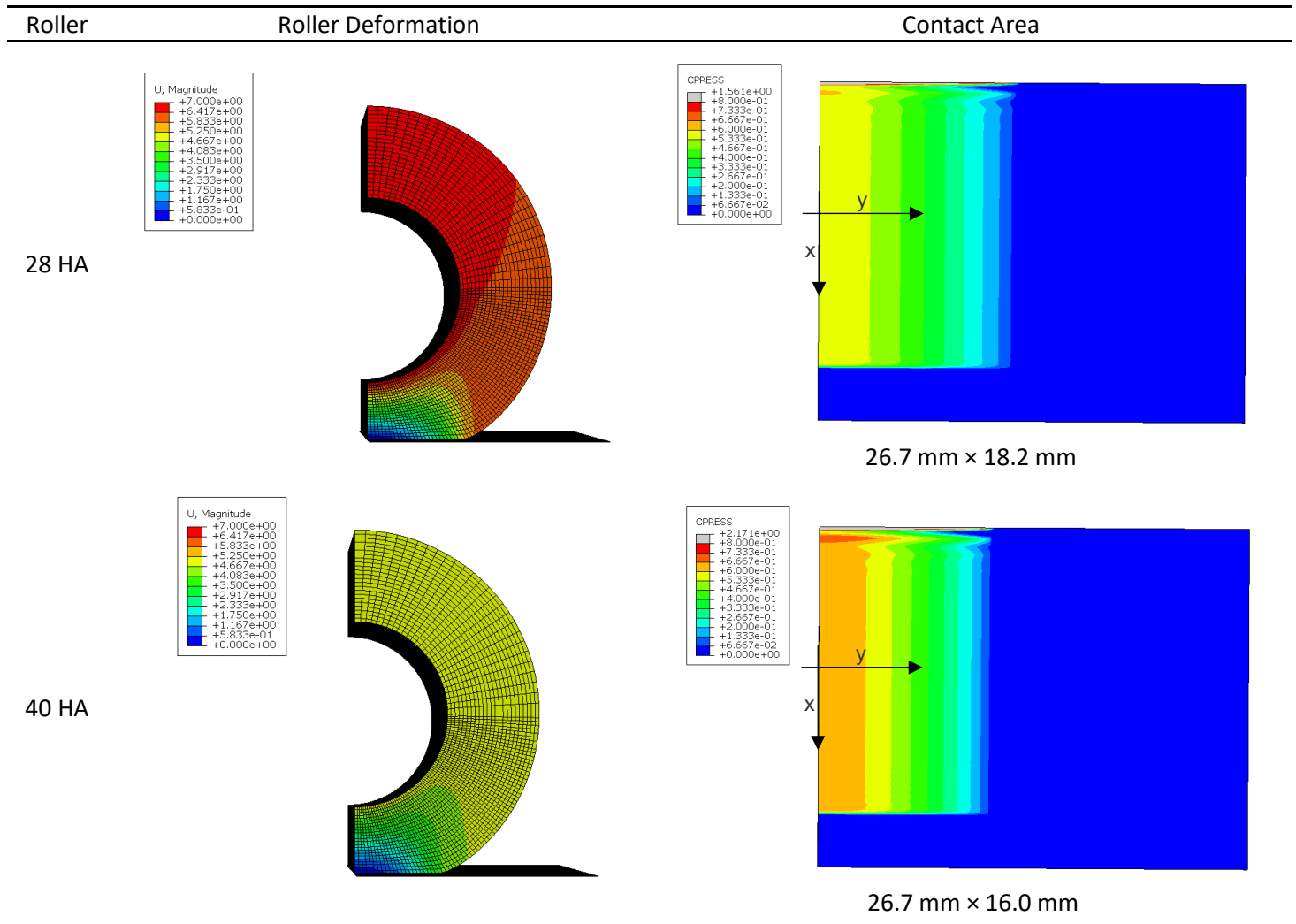
Influence of tool curvature on compaction pressure

Figure 13 shows the compaction pressure distribution along the x-direction under a compaction force of 600 N generated by the two softer rollers on both a flat tool and the curved tools. A pressure spike is observed at the edge of the contact area which was also found in the compacted pressure sensitive film. It is shown that for flat tools, the compaction pressure is uniform except in the pressure spike area for both rollers and that the pressure generated by the 40 HA roller is higher than that generated by the 28 HA one. Whilst for the convex tools, the compaction pressure has a convex shape and the shape becomes more pronounced when decreasing the radius of curvature. 40 HA roller has a less uniform compaction distribution than the 28 HA roller under the same radius of curvature.

Figure 14 shows the influence of radius of curvature on the pressure uniformity under a compaction force of 600 N. Pressure uniformity is calculated from the nodes on the tow 3 and tow 4 shown in Figure 6 (b) to avoid the influence of the local pressure spike. It is shown that the 28 HA roller has higher pressure uniformity than the 40 HA roller under the same radius of curvature, which is in agreement with the observations in Figure 11. For both rollers, the pressure uniformity decreases slightly with an increase of curvature when radius of curvature is higher than 100 mm before decreasing dramatically for radii smaller than 100 mm.
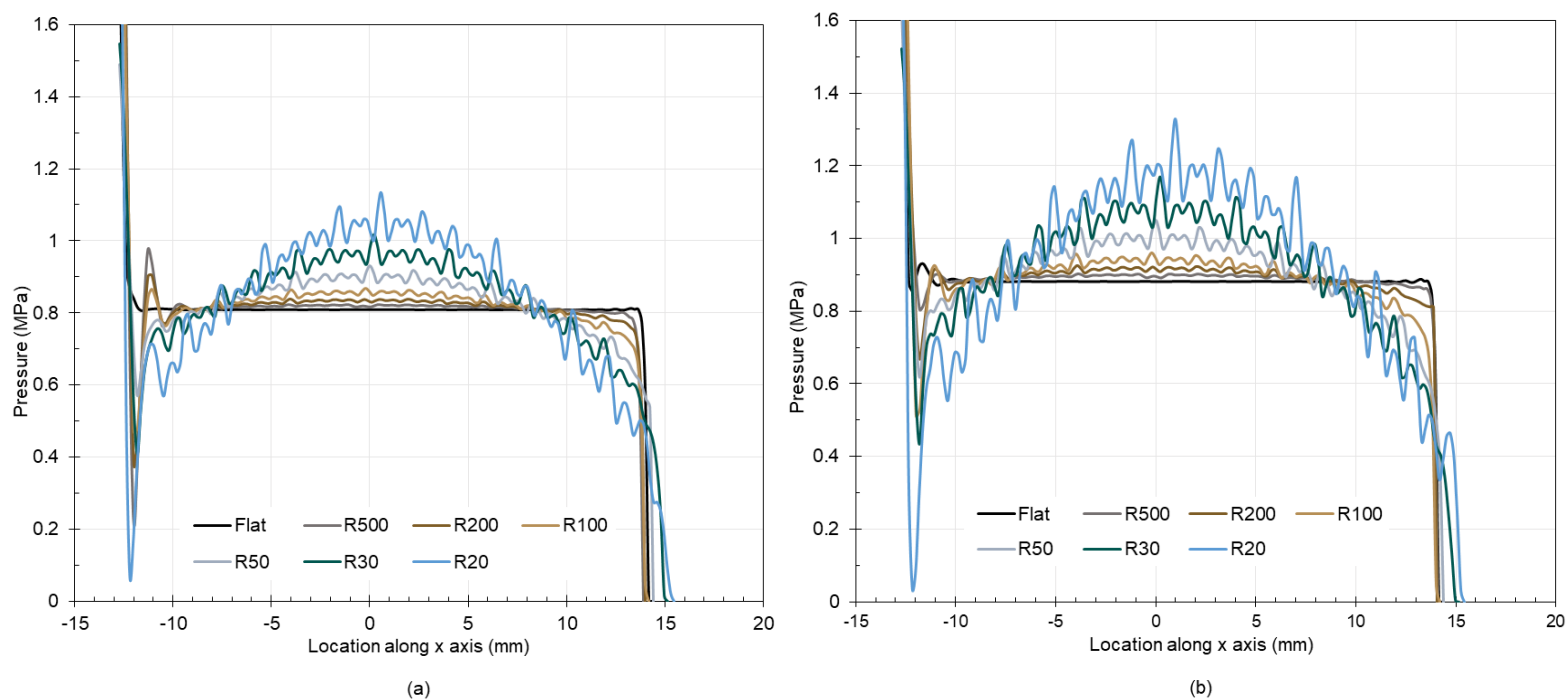
Figure 13 Simulated compaction pressure distribution of (a) 28 HA roller and (b) 40 HA roller on curved surfaces under a compaction force of 600 N (0 in x axis is positioned at the boundary between tow 2 and tow 3)
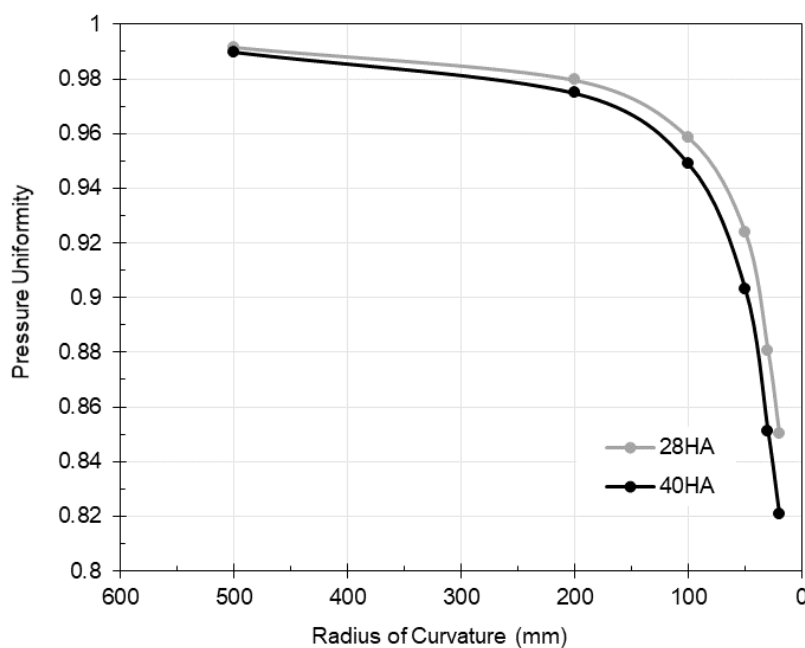
Figure 14 Pressure uniformity (calculated using equation (8) for tow 3 and tow 4) of two rollers on curved surfaces under a compaction force of 600 N

Target force windows of rollers on curved tools

In other research on roller compaction on curved tools, the pressure uniformity given by different compaction rollers was compared for the same applied force. However, the pressure generated by different hardness rollers vary under the same applied force (due to the difference in effective contact area). In this work the pressure uniformity is found to depend on the force input according to the curves shown in Figure 15. For both rollers, pressure uniformity increases monotonically with the applied compaction force. At a low level of compaction force, the rate of increase is almost constant but this then decreases more gradually above 200N. In this research, instead of comparing the pressure uniformity of two rollers under the same force input, force 'windows' of the two rollers are determined for curved tools to satisfy the compaction pressure requirement (between 0.5 MPa and 0.9 MPa), to ensure good consolidation of the bindered tape without excessive force.
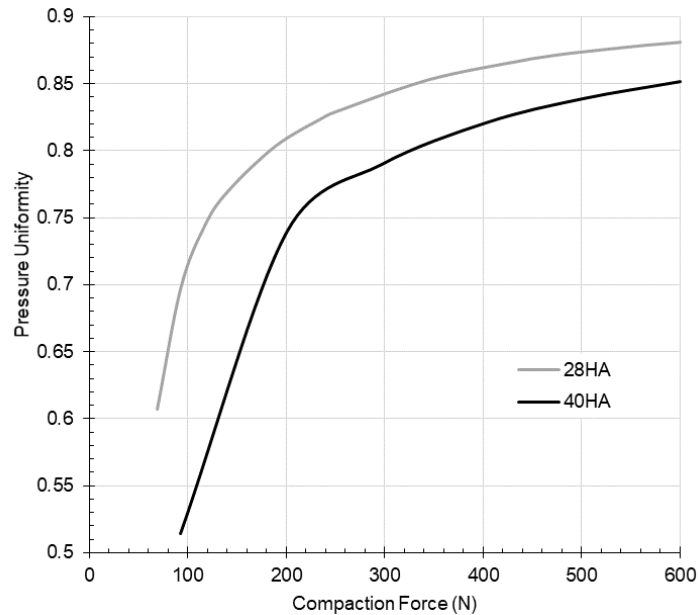
Figure 15 Influence of compaction force on pressure uniformity (calculated using equation (8) for tow 3 and tow 4) for roller compaction on the tool with radius of curvature of 30 mm

Figure 16 shows the influence of applied force on the maximum and minimum contact pressure between the roller and the dry fibre substrate for the 28 HA roller on a tool with a radius of 30 mm. The maximum and minimum pressures are calculated from nodes in tow 3 and tow 4 as shown in Figure 6 (b) to avoid the influence of the pressure spike. It is found that maximum and minimum pressure shows a linear relationship with compaction force when the force is higher than 200 N. The other compaction results on different tool curvatures and roller materials show similar trends. The target force window is obtained from the intersection points of maximum and minimum pressure curves with the target pressure requirement bounds. Target force window results for other combinations are shown in Table 6. The maximum force applied in the FE simulation is 600 N but in reality, the actual upper bound of force which satisfies the compaction pressure requirement is above 600 N for 28 HA roller compaction on tools with radius of curvature greater than 100 mm. It is found that neither roller meets the pressure requirement for tools with radius of curvature of 20 mm, but the 28 HA roller can satisfy the requirement for a radius of curvature of 30 mm while the 40 HA roller cannot. For tools with other curvatures, 28 HA roller has a larger force window than the 40 HA roller. These force windows provide guidance for the force control of the ADFP process and it is recommended that forces toward the upper end of the acceptable range should be chosen for force input since the pressure uniformity has been shown to increase with increasing compaction force.
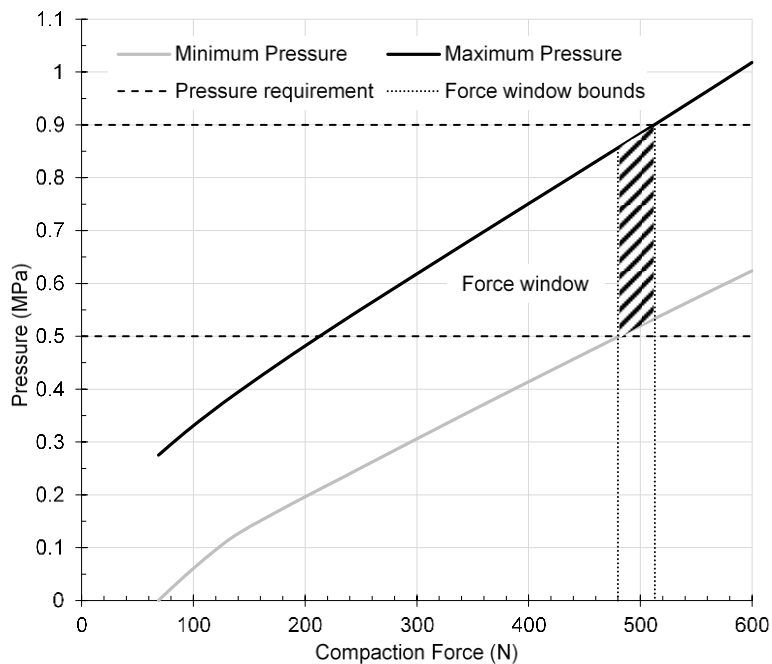
Figure 16 Influence of compaction force on maximum and minimum observed contact pressure between 28 HA roller and the tool with radius of curvature of 30 mm

Table 6 Force windows for tools with different curvatures

Radius of Curvature (mm)	28 HA Roller	40 HA Roller
20	-	-
30	480-513 N	-
50	435-563 N	447-492 N
100	398-600* N	350-538 N
200	347-600* N	320-557 N
500	338-600* N	304-597 N

*Actual upper bound is larger than 600 N.

Influence of substrate thickness
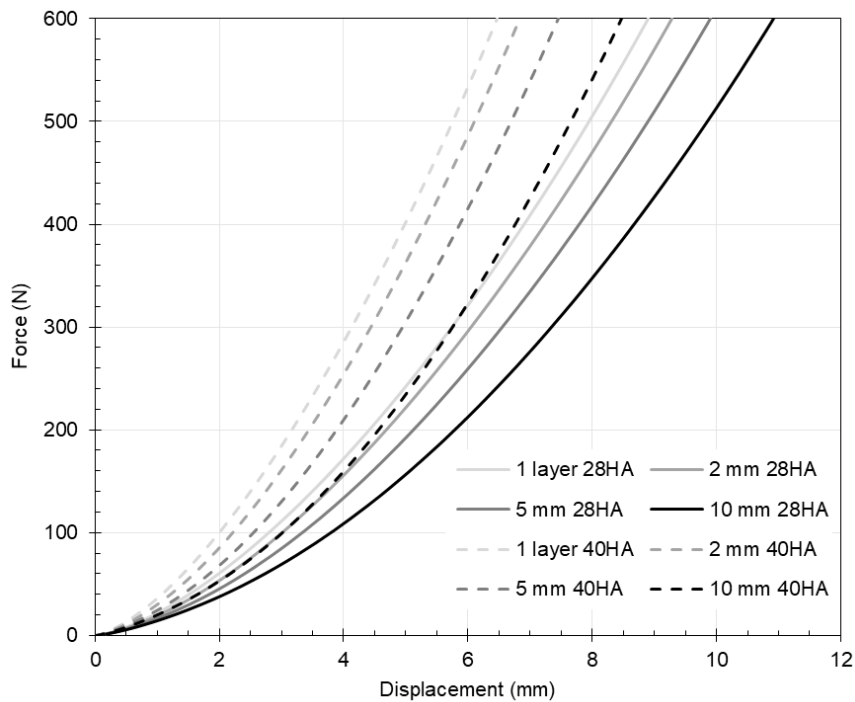
Figure 17 Load displacement curves for two compaction rollers on dry fibre substrates with different thickness (Displacement consists of the deformation of rollers and dry fibre substrates)

The simulation results show that the thickness of dry fibre substrate has minimal influence on compaction pressure since uniform material properties are used in this model for the dry fibre substrate. However, different layers of dry fibres have different compaction properties due to their different compaction history [37, 39]. The cyclic properties of carbon fibre are beyond the scope of this research and the model will be improved to consider the non-uniform properties of thick dry fibre substrates in the future. Thick dry fibre substrates exhibit large deformation which is greater than twice the deformation of thermoset prepregs in the AFP process as discussed in the introduction. This larger deformation leads to larger displacement of the roller during the deposition process as shown in Figure 17. This larger displacement potentially complicates force control. If a position/displacement-based control strategy is used and the large displacement of the 10 mm dry fibre substrate is not considered, a force error around 43% can be produced. Thus, a force-based control strategy instead of position/displacement-based control strategy should be used for ADFP. Commercial deposition hardware deals with this issue by including some kind of built-in compliance (often in the form of a pneumatic cylinder) in order to maintain a roughly constant compaction force. The method developed here to use a target force window, when combined with real-time force feedback and knowledge of local tool geometry has the potential improve the quality of preforms by having tighter control over height and force.

5.Conclusion

An experimentally validated roller compaction on dry carbon fibres model has been built in this research. The model has been used to investigate the influence of roller material, tool curvature and substrate thickness on the compaction pressure in the ADFP process. The following conclusions are obtained:

The force applied by the deposition head when using different roller materials should be adjusted to obtain equivalent compaction pressure on the preform in order to optimise the binder performance in the finished preform. Harder

rollers generate smaller contact areas and greater pressure non-uniformity. Precise force control is more challenging for harder rollers due to their very low displacement under compaction.

For deposition on curved tools, compaction pressure uniformity decreases with increasing tool curvature for a given force. However, for a given curvature, pressure uniformity is directly proportional to applied force. Target force windows for roller compaction on tools with different curvatures have been obtained. Softer rollers exhibit larger force control window and increased suitability for tools with larger curvature. Given the high influence of tool curvature on required force, *a priori* knowledge of the tool curvature could significantly improve preform quality. This will be the subject of future work.

Thick dry fibre substrates exhibit large deformation under compaction during the ADFP process which brings complexity to the force control strategy. If an improper control strategy is used and the large deformation of thick dry fibre substrates is disregarded, a force error up to 43% can be generated.

These results provide guidance for the choices of roller and force control strategy for ADFP process. In common with existing research on AFP, it is recommended that complaint rollers should be used in ADFP process because they are more applicable for precise force control and deposition on curved tools. Target force windows for roller compaction on curved tools provide force control input for ADFP. A force-based control strategy instead of a position-based control strategy is recommended for ADFP process especially for deposition on thick dry fibre substrates.

Declaration of Competing Interest
The authors declare that they have no known competing financial interests or personal relationships that could have appeared to influence the work reported in this paper.

Author Contributions
Shimin Lu: Conceptualization, Methodology, Software, Validation, Data curation, Formal analysis, Investigation, Visualization, Writing – original draft. **Anthony Evans**: Resources, Validation, Supervision, Writing – review & editing. **Thomas Turner**: Conceptualization, Funding acquisition, Project administration, Resources, Supervision, Writing - review & editing.

Data Availability
The raw/processed data required to reproduce these findings cannot be shared at this time as the data also forms part of an ongoing study.

References
[1] Lukaszewicz DHJA, Ward C, Potter KD. The engineering aspects of automated prepreg layup: History, present and future. Composites Part B: Engineering. 2012;43:997-1009.
[2] Endruweit A, Ghose S, Johnson BA, Kelly S, De Focatiis DS, Warrior NA. Tack testing to Aid Optimisation of Process Parameters for Automated Material Placement in an Industrial Environment. Annual International Conference on Composite Materials (ICCM 21), Xi'an2017. p. 20-5.
[3] Endruweit A, Choong GYH, Ghose S, Johnson BA, Younkin DR, Warrior NA, et al. Characterisation of tack for uni-directional prepreg tape employing a continuous application-and-peel test method. Composites Part A: Applied Science and Manufacturing. 2018;114:295-306.
[4] Rao S, Umer R, Thomas J, Cantwell WJ. Investigation of peel resistance during the fibre placement process. Journal of Reinforced Plastics and Composites. 2015;35:275-86.
[5] Budelmann D, Detampel H, Schmidt C, Meiners D. Interaction of process parameters and material properties with regard to prepreg tack in automated lay-up and draping processes. Composites Part A: Applied Science and Manufacturing. 2019;117:308-16.
[6] Zhao P, Shirinzadeh B, Shi Y, Cheuk S, Clark L. Improved uniform degree of multi-layer interlaminar bonding strength for composite laminate. Journal of Reinforced Plastics and Composites. 2017;36:1211-24.

[7] Zhao P, Shirinzadeh B, Shi Y, Cheuk S, Clark L. Multi-pass layup process for thermoplastic composites using robotic fiber placement. Robotics and Computer-Integrated Manufacturing. 2018;49:277-84.

[8] Tierney J, Gillespie JW. Modeling of In Situ Strength Development for the Thermoplastic Composite Tow Placement Process. Journal of Composite Materials. 2006;40:1487-506.

[9] Khan MA, Mitschang P, Schledjewski R. Identification of some optimal parameters to achieve higher laminate quality through tape placement process. Advances in Polymer Technology. 2010;29:98-111.

[10] Oromiehie E, Prusty GB, Compston PP, Rajan G. The influence of consolidation force on the performance of AFP manufactured laminates. 21st International Conference on Composite Materials (ICCM-21). Xi'an2017.

[11] Liu X, Qian S, Ye Y, Xu Q, Li X. Effect of process parameters on mode-II interlaminar fracture toughness and fractographic features of automated fibre placement prepreg laminates. Journal of Composite Materials. 2021.

[12] Miao Q, Dai Z, Ma G, Niu F, Wu D. Effect of consolidation force on interlaminar shear strength of CF/PEEK laminates manufactured by laser-assisted forming. Composite Structures. 2021;266.

[13] Oromiehie E, Gain AK, Prusty BG. Processing parameter optimisation for automated fibre placement (AFP) manufactured thermoplastic composites. Composite Structures. 2021;272.

[14] Khan MA, Mitschang P, Schledjewski R. Parametric study on processing parameters and resulting part quality through thermoplastic tape placement process. Journal of Composite Materials. 2013;47:485-99.

[15] Bakhshi N, Hojjati M. Effect of compaction roller on layup quality and defects formation in automated fiber placement. Journal of Reinforced Plastics and Composites. 2019.

[16] Cheng J, Zhao D, Chen H, Zhang Y, Wang Y. Effect of the attitude fine-adjustment of compaction roller on automated fiber placement defects and trajectory. Journal of Reinforced Plastics and Composites. 2019.

[17] Jiang J, He Y, Ke Y. Pressure distribution for automated fiber placement and design optimization of compaction rollers. Journal of Reinforced Plastics and Composites. 2019.

[18] Ammar MMA, Shirinzadeh B. The Role of Compaction Roller in Defining the Layup Quality and Laminate Porosity in Robotic Fiber Placement. 2021 24th International Conference on Mechatronics Technology (ICMT)2021. p. 1-6.

[19] Chu Q, Li Y, Xiao J, Huan D, Zhang X. Placeability restricted by in-complete contact between laying roller and mould in an automated fiber placement process. Journal of Reinforced Plastics and Composites. 2018;37:475-89.

[20] Lichtinger R, Lacalle J, Hinterhölzl R, Beier U, Drechsler K. Simulation and experimental validation of gaps and bridging in the automated fiber placement process. Science and Engineering of Composite Materials. 2015;22.

[21] Qu W, He R, Cheng L, Yang D, Gao J, Wang H, et al. Placement suitability analysis of automated fiber placement on curved surfaces considering the influence of prepreg tow, roller and AFP machine. Composite Structures. 2021;262.

[22] Jiang J, He Y, Wang H, Ke Y. Modeling and experimental validation of compaction pressure distribution for automated fiber placement. Composite Structures. 2021;256.

[23] He Y, Jiang J, Qu W, Ke Y. Compaction pressure distribution and pressure uniformity of segmented rollers for automated fiber placement. Journal of Reinforced Plastics and Composites. 2021.

[24] Sloan J. Infused wing sheds light on aerocomposites future. Composites World2018.

[25] Kadiyala AK, Portela A, Devlin K, Lee S, O'Carroll A, Jones D, et al. Mechanical evaluation and failure analysis of composite laminates manufactured using automated dry fibre tape placement followed by liquid resin infusion. Composites Science and Technology. 2021;201.

[26] Liu YN, Yuan C, Liu C, Pan J, Dong Q. Study on the resin infusion process based on automated fiber placement fabricated dry fiber preform. Sci Rep. 2019;9:7440.

[27] Assadi M, Field T. AFP Processing of Dry Fiber Carbon Materials (DFP) for Improved Rates and Reliability. SAE Technical Paper Series2020.

[28] Kelly PA. Transverse compression properties of composite reinforcements. Composite Reinforcements for Optimum Performance: Elsevier Ltd; 2011. p. 333-66.

[29] Di Francesco M. Laser-assisted Automated Fibre Placement Process Development [EngD Thesis]: University of Bristol, 2017.

[30] Veldenz L. Automated Dry Fibre Placement and Infusion Process Development for Complex Geometries [EngD Thesis]: University of Bristol, 2019.

[31] Nixon-Pearson OJ, Belnoue J-H, Ivanov DS, Potter KD, Hallett SR. An experimental investigation of the consolidation behaviour of uncured prepregs under processing conditions. Journal of Composite Materials. 2016;51:1911-24.

[32] Veldenz L, Di Francesco M, Giddings P, Kim BC, Potter K. Material selection for automated dry fiber placement using the analytical hierarchy process. Advanced Manufacturing: Polymer & Composites Science. 2019;4:83-96.

[33] Çelik O, Peeters D, Dransfeld C, Teuwen J. Intimate contact development during laser assisted fiber placement: Microstructure and effect of process parameters. Composites Part A: Applied Science and Manufacturing. 2020;134.

[34] Evans AD, Turner TA, Endruweit A. Development of Automated Dry Fibre Placement for High Rate Deposition. 22nd International Conference on Composite Materials (ICCM22). Melbourne2019.

[35] Lin H, Sherburn M, Crookston J, Long AC, Clifford MJ, Jones IA. Finite element modelling of fabric compression. Modelling and Simulation in Materials Science and Engineering. 2008;16.

[36] Sherburn M. Geometric and Mechanical Modelling of Textiles: University of Nottingham, 2007.

[37] Lectez A-S, El Azzouzi K, Binetruy C, Comas-Cardona S, Verron E, Lebrun J-M. Three-dimensional mechanical properties of dry carbon fiber tows subjected to cyclic compressive loading. Journal of Composite Materials. 2018;52:2661-77.

[38] Dharmalingam AS, Hemmer J, Lectez AS, Binetruy C, Comas-Cardona S. Evolution of single carbon and glass fibrous tow cross-sections in dry and lubricated states during compaction perpendicular to the fibers. Composites Part B: Engineering. 2018;148:235-42.

[39] Kabachi MA, Danzi M, Arreguin S, Ermanni P. Experimental study on the influence of cyclic compaction on the fiber-bed permeability, quasi-static and dynamic compaction responses. Composites Part A: Applied Science and Manufacturing. 2019;125.

Figure captions

Figure 1 Carbon fibre tapes used in this paper showing upper and lower surfaces (1 mm minor grid spacing)

Figure 2 Compaction roller (a) Manufactured roller (b) Cross-section view of roller in CAD

Figure 3 Dry fibre tape compaction testing experimental apparatus

Figure 4 Compaction curve of carbon fibre tapes from experimental results with power law fitted curve

Figure 5 Compaction roller with fixture

Figure 6 Experimental setup for compaction on fibres test (a) machine setup (b) illustration of the relative location of the roller and fibre tows

Figure 7 Pressure film and pressure results (a) scanning picture of pressure sensitive film (b) calculated pressure values from Matlab

Figure 8 Averaged pressure results along tow centreline in y direction (the dash line in Figure 7) from pressure sensitive film

Figure 9 FE model setup for roller compaction on a layer of dry carbon fibre

Figure 10 FE Model setup of roller compaction on dry carbon fibre with single curvature tools

Figure 11 Load displacement curves of three rollers from experimental and FE results (experimental curves show upper and lower bounds based on four repeats)

Figure 12 Compaction pressured distribution along tow centreline in y axis from experimental and FE results (a) 28HA roller (b) 40HA roller

Figure 13 Simulated compaction pressure distribution of (a) 28HA roller and (b) 40HA roller on curved surfaces under a compaction force of 600 N (0 in x axis is positioned at the boundary between tow 2 and tow 3)

Figure 14 Pressure uniformity (calculated using equation (8) for tow 3 and tow 4) of two rollers on curved surfaces under a compaction force of 600 N

Figure 15 Influence of compaction force on pressure uniformity (calculated using equation (8) for tow 3 and tow 4) for roller compaction on the tool with radius of curvature of 30 mm

Figure 16 Influence of compaction force on maximum and minimum observed contact pressure between 28HA roller and the tool with radius of curvature of 30 mm

Figure 17 Load displacement curves for two compaction rollers on dry fibre substrates with different thickness (Displacement consists of the deformation of rollers and dry fibre substrates)

Table captions

Table 1 Forces used to determine compaction behaviour

Table 2 Input values for the material model of the dry fibre tapes

Table 3 Material properties for the rollers

Table 4 Compaction pressure distribution results under three different load level for three rollers

Table 5 Simulation results of the roller deformation and the contact area of 28HA, 40HA roller under a compaction force of 400 N

Table 6 Force windows for tools with different curvatures